Appl Nanosci (2017) 7:209–214
DOI 10.1007/s13204-017-0566-y

ORIGINAL ARTICLE

Synthesis and magnetic induction heating properties of Gd-substituted Mg–Zn ferrite nanoparticles

Fumie Hirosawa[1] · **Tomohiro Iwasaki**[1] · **Satoru Watano**[1]

Received: 2 March 2017 / Accepted: 17 April 2017 / Published online: 19 April 2017

Abstract Gadolinium-substituted magnesium–zinc ferrite ($Mg_xZn_{1-x}Gd_yFe_{2-y}O_4$) nanoparticles with different metal compositions for x between 0 and 1 and y between 0 and 0.06 were synthesized via coprecipitation of metal hydroxides, followed by calcination. Their crystal structure was characterized via X-ray diffraction analysis, confirming that the Gd-substituted Mg–Zn ferrite samples had a single-phase spinel structure. The metal composition significantly affected the crystal structure, including the lattice parameters and crystallite size. Scanning electron microscopy (SEM) showed that the ferrite samples had a diameter of approximately 50–200 nm. Furthermore, the temperature rise in an alternating magnetic field was measured, and the magnetic induction heating properties were evaluated using the specific absorption rate (SAR) determined from the temperature profile. The SAR significantly varied depending on the compositions of x and y. When $x = 0.5$ and $y = 0.02$, the SAR was found to be at maximum. This reveals that the compositions can control the magnetic induction heating properties. The results suggest that Gd-substituted Mg–Zn ferrite nanoparticles are promising candidates for magnetic hyperthermia applications.

Keywords Magnesium–zinc ferrites · Gadolinium substitution · Induction heating · Hyperthermia

Introduction

Magnesium–zinc (Mg–Zn) ferrites ($Mg_xZn_{1-x}Fe_2O_4$, $0 < x < 1$) are well known as a soft magnetic material with good properties, such as electrical resistivity (Ali et al. 2017; Mansour and Abdo 2017; Sharma et al. 2016), low eddy current loss at high frequencies (Mansour and Abdo 2017; Sharma et al. 2016), and induction heating properties in an alternating (AC) magnetic field (El-Sayed et al. 2017; Reyes-Rodríguez et al. 2017), and they are widely used in various industrial products, e.g., power transformers (Choodamani et al. 2016; Sharma et al. 2016), microwave devices (Choodamani et al. 2016; Ghodake et al. 2017; Sharma et al. 2016), and telecommunications equipment (Choodamani et al. 2016; Ghodake et al. 2017). In recent years, the biocompatibility of Mg–Zn ferrites has also attracted attention, and several researchers have studied their application as a heating mediator in magnetic hyperthermia treatments (Ali et al. 2017; El-Sayed et al. 2017; Reyes-Rodríguez et al. 2017). To use Mg–Zn ferrites for magnetic hyperthermia, the induction heating behavior must be precisely controlled. As a promising means for controlling the properties, the metal composition of ferrites has often been adjusted. For example, when the Mg/Zn molar ratio in an Mg–Zn ferrite is varied, the generation of heat can be controlled due to variations of the magnetic properties such as magnetization (El-Sayed et al. 2017; Reyes-Rodríguez et al. 2017). Furthermore, the replacement of Fe^{3+} ions in the ferrite structure with other metal ions has also been performed to vary the magnetization. In particular, gadolinium (Gd) is a frequently used transition metal for the replacement because of its large magnetic moment, magneto-crystalline anisotropy, magnetostriction (Kumar et al. 2014), and biocompatibility (Chaudhary et al. 2015; Elkady et al. 2015). In prior studies (Elkady et al.

✉ Tomohiro Iwasaki
iwasaki@chemeng.osakafu-u.ac.jp

[1] Department of Chemical Engineering, Osaka Prefecture University, Sakai, Osaka 599-8531, Japan

2015; Hejase et al. 2012; Raja et al. 2017; Yao et al. 2009), the replacement of Fe^{3+} ions with Gd^{3+} ions in Mg ferrites and Zn ferrites was performed, resulting in a variation of their magnetization. This led to enhanced performance for magnetic hyperthermia mediators (Elkady et al. 2015; Hejase et al. 2012; Raja et al. 2017; Yao et al. 2009) and magnetic resonance imaging (MRI) contrast agents (Elkady et al. 2015; Raja et al. 2017). Accordingly, the Gd substitution in Mg–Zn ferrites can not only maintain the biocompatibility of the ferrites but also contribute to the control of induction heating behavior. However, to our knowledge, there have been no reports on the induction heating properties of Gd-substituted Mg–Zn ferrites.

Therefore, in this work, we studied the synthesis of Gd-substituted Mg–Zn ferrites and the composition dependence of magnetic induction heating properties to provide criteria for the preparation of materials available for magnetic hyperthermia.

Experimental

Synthesis

Gd-substituted Mg–Zn ferrite ($Mg_xZn_{1-x}Gd_yFe_{2-y}O_4$) nanoparticles with different compositions of x ($x = 0$, 0.25, 0.5, 0.75 and 1) and y ($y = 0$, 0.02, 0.04 and 0.06) were synthesized via calcination of a precursor consisting of metal hydroxides prepared via coprecipitation. Metal chloride solutions with a concentration of 0.1 M were separately prepared by dissolving $MgCl_2{\cdot}6H_2O$, $ZnCl_2$, $GdCl_3{\cdot}6H_2O$, and $FeCl_3{\cdot}6H_2O$ (Wako Pure Chemical Industries) into deionized water. When preparing the $ZnCl_2$ solution, a tiny amount of 36.6 mass % HCl solution was added to the solution to completely dissolve $ZnCl_2$. Predetermined amounts of the metal chloride solutions corresponding to x and y were mixed and stirred for 10 min with a magnetic stirrer. Afterwards, a 1 M NaOH solution was slowly added to the mixed solution at a rate of approximately 1 g/min under stirring. According to the following reaction, a mixture of the metal hydroxides was formed:

$$x\mathrm{MgCl_2} + (1-x)\mathrm{ZnCl_2} + y\mathrm{GdCl_3} + (2-y)\mathrm{FeCl_3} + 8\mathrm{NaOH} \rightarrow x\mathrm{Mg(OH)_2} + (1-x)\mathrm{Zn(OH)_2} + y\mathrm{Gd(OH)_3} + (2-y)\mathrm{Fe(OH)_3} + 8\mathrm{NaCl}. \quad (1)$$

The final molar ratio of $OH^-/(Mg^{2+} + Zn^{2+} + Gd^{3+} + Fe^{3+})$ in the resulting solution was fixed at 8/3, and the pH was higher than 12 regardless of x and y. The solution was vigorously stirred for an additional 30 min. The precipitates were separated from the solution by centrifugation, washed with water for removing NaCl, and dried at 383 K for longer than 12 h. The precursor obtained was ground using a mortar and pestle and calcined at 1173 K for 5 h in the air. Finally, the $Mg_xZn_{1-x}Gd_yFe_{2-y}O_4$ ferrites were formed according to the following reaction:

$$x\mathrm{Mg(OH)_2} + (1-x)\mathrm{Zn(OH)_2} + y\mathrm{Gd(OH)_3} + (2-y)\mathrm{Fe(OH)_3} \rightarrow \mathrm{Mg_xZn_{1-x}Gd_yFe_{2-y}O_4} + 4\mathrm{H_2O}. \quad (2)$$

In addition, the precursor with the composition of $x = 0.5$ and $y = 0.02$ was also calcined at 973 and 1073 K to obtain samples with different crystallinities.

Characterization

The phase evolution and crystallinity of the samples were evaluated using a powder X-ray diffractometer (XRD; RINT-1500, Rigaku, Cu Kα radiation, 40 kV, 80 mA). The average crystallite size, D, was calculated via Scherrer's equation (Eq. 3) using the diffraction data measured at $2\theta \approx 30.1°$, 35.4°, and 62.6°, which corresponded to the (220), (311), and (440) planes, respectively:

$$D = K\lambda/(\beta\cos\theta) \quad (3)$$

where K is the Scherrer constant, β is the integral breadth of the peak, λ is the X-ray wavelength, and θ is the diffraction angle. The a-axis lattice constant, a, was also determined using Eq. 4 from the XRD data measured at the (220), (311), and (440) planes, and the average was calculated:

$$a = d_{hkl}(h^2 + k^2 + l^2)^{0.5} \quad (4)$$

where h, k, and l are the Miller indices (h k l) and d_{hkl} is the interplanar spacing. Furthermore, the morphology was observed with a field emission scanning electron microscope (FE-SEM; JSM-6700F, JEOL, 18.0 kV).

The induction heating properties of magnetic fluids consisting of the sample powder (5 mass %) and glycerol (Smolkova et al. 2015) were evaluated using an AC magnetic field generator composed of a radio frequency power source (T162-5723A, THAMWAY), an impedance matching box (T020-5723F, THAMWAY), and a solenoid coil (70 mm in inner diameter) with 21 turns of copper tube (4 mm in outer diameter and 3 mm in inner diameter). Cooling water flowed inside the copper tube. One milliliter of the magnetic fluid was charged in a glass test tube with an outer diameter of 15 mm. After sonication, the test tube was placed in the center of the coil. The temperature rise of the fluid in the AC magnetic field was measured with an optical fiber thermometer (FTI-10 with FOT-L-NS-967, FISO Technologies). The frequency and amplitude of the magnetic field were 600 kHz and 5 kA/m, respectively

(Hirosawa et al. 2016). The specific absorption rate (SAR) corresponding to the heat generation of the sample powder, defined by Eq. 5, was determined (El-Sayed et al. 2017; Reyes-Rodríguez et al. 2017):

$$\mathrm{SAR} = [\{mC_{\mathrm{pf}} + (1-m)C_{\mathrm{pg}}\}/m](\Delta T/\Delta t) \quad (5)$$

where m is the content of the sample powder in the fluid (i.e., $m = 0.05$), C_{pf} (=0.61–0.75 J/(g K) (Hajarpour et al. 2013; Klemme and Ahrens 2005)) and C_{pg} (=2.43 J/(g K) (Smolkova et al. 2015)) are the specific heat capacities of ferrite and glycerol, respectively, T is the temperature, t is the time, and $\Delta T/\Delta t$ is the initial heating rate.

Results and discussion

Characterization

Figure 1 shows the XRD patterns of $Mg_xZn_{1-x}Gd_yFe_{2-y}O_4$. The samples were confirmed to have a single-phase spinel structure except for the Zn ferrite ($ZnGd_{0.06}Fe_{1.94}O_4$) and Mg ferrite ($MgGd_yFe_{2-y}O_4$; $y = 0.02$, 0.04, and 0.06) samples containing gadolinium orthoferrite ($GdFeO_3$) as the by-product. This result demonstrates that our synthesis method can provide Gd-substituted Mg–Zn ferrites, whereas Fe^{3+} ion in Zn ferrites and Mg ferrites is difficult to replace with Gd^{3+} ions. As shown in Fig. 2, the lattice parameter, a, tended to decrease with increasing Mg content, x, because the ionic radius of the Mg^{2+} ion (0.66 Å) is smaller than that of the Zn^{2+} ion (0.82 Å) (El-Sayed et al. 2017; Reyes-Rodríguez et al. 2017). In contrast, the Gd content, y, hardly affected the lattice parameter due to the relatively low Gd replacement. Figure 3 illustrates the variation in the average crystallite size, D, with the Mg content, x, and Gd content, y. The average crystallite size slightly increased with decreasing Mg content at relatively low Gd contents ($y = 0$–0.04), because the diffusion of Zn^{2+} ions in the crystal lattice may slightly expand the lattice spacing (Gao et al. 2015). In addition, the crystallite size tended to decrease with increasing Gd content because of the inhibition of grain growth due to the incorporation of Gd^{3+} ions into the ferrite structure (Haralkar et al. 2012). However, when $y = 0.06$, the Gd-substituted Zn ferrite

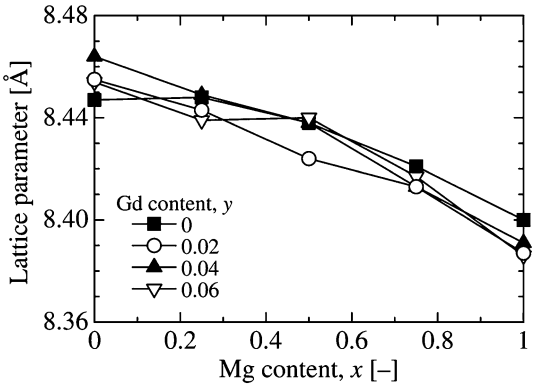

Fig. 2 Variation of the a-axis lattice parameter of $Mg_xZn_{1-x}Gd_yFe_{2-y}O_4$ calcined at 1173 K

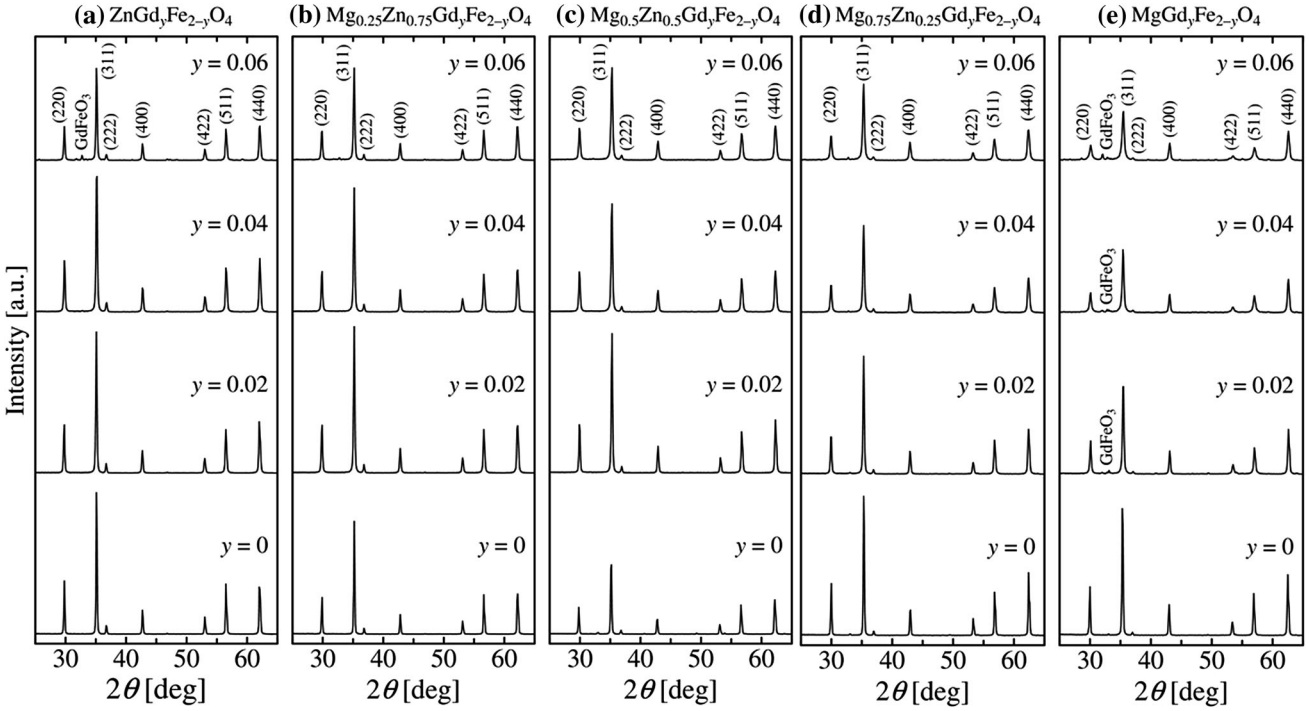

Fig. 1 XRD patterns of $Mg_xZn_{1-x}Gd_yFe_{2-y}O_4$ with $x =$ **a** 0, **b** 0.25, **c** 0.5, **d** 0.75, and **e** 1 calcined at 1173 K

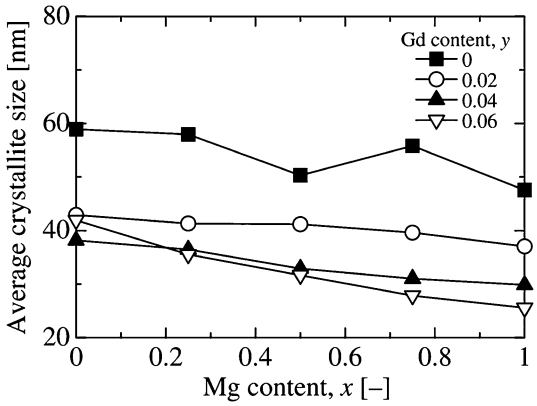

Fig. 3 Variation of the average crystallite size of $Mg_xZn_{1-x}Gd_y$-$Fe_{2-y}O_4$ calcined at 1173 K

($x = 0$) sample had a relatively large crystallite size. As shown in Fig. 1, this sample contained a small amount of $GdFeO_3$, which may lead to a surplus of Zn^{2+} ions in the ferrite structure, resulting in expansion of the lattice spacing as mentioned earlier.

Figure 4 shows a typical SEM image of $Mg_{0.5}Zn_{0.5}$-$Gd_{0.02}Fe_{1.98}O_4$ nanoparticles calcined at 1173 K. The particle diameter was approximately 50–200 nm, indicating that the nanoparticles were polycrystalline. For other x and y contents, similar results were obtained.

Induction heating properties

Figure 5 shows the typical temperature profiles of the magnetic fluids containing the $Mg_{0.5}Zn_{0.5}Gd_yFe_{2-y}O_4$ nanoparticles. The temperature of the magnetic fluids rapidly increased immediately after applying the magnetic field. Figure 6 illustrates the composition dependence of

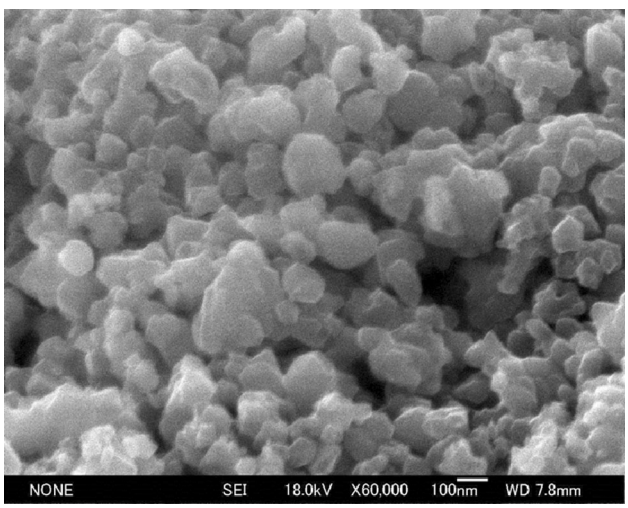

Fig. 4 Typical SEM image of $Mg_{0.5}Zn_{0.5}Gd_{0.02}Fe_{1.98}O_4$ calcined at 1173 K

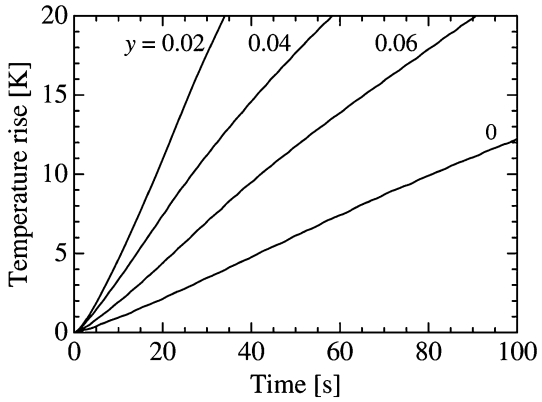

Fig. 5 Typical temperature profile curves of $Mg_{0.5}Zn_{0.5}Gd_yFe_{2-y}O_4$

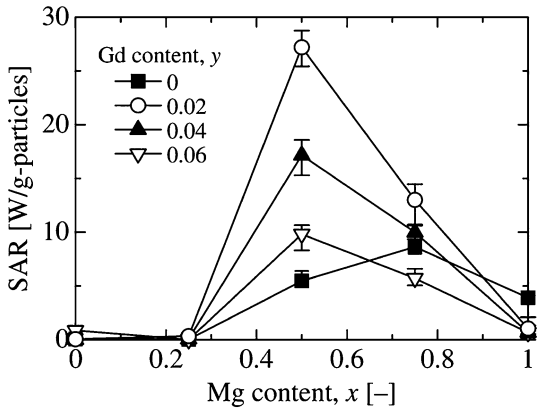

Fig. 6 Composition dependence of the SAR of $Mg_xZn_{1-x}Gd_yFe_{2-y}$-O_4 calcined at 1173 K

the SAR. When $y = 0$ (i.e., $Mg_xZn_{1-x}Fe_2O_4$), the maximum value of the SAR was observed at $x = 0.75$. This can be explained by the magnetization and coercivity of the samples. According to Choodamani et al. (2016), the coercivity of $Mg_{0.75}Zn_{0.25}Fe_2O_4$ was approximately three times as large as that of $Mg_{0.5}Zn_{0.5}Fe_2O_4$, although they had a similar level of magnetization. In addition, the magnetization of $MgFe_2O_4$ was approximately half of those of $Mg_{0.5}Zn_{0.5}Fe_2O_4$ and $Mg_{0.75}Zn_{0.25}Fe_2O_4$. Therefore, the $Mg_{0.75}Zn_{0.25}Fe_2O_4$ sample showed a larger hysteresis loss in the magnetic field, resulting in a higher heat generation. When a small amount of Fe^{3+} ions was replaced with Gd^{3+} ions, i.e., at $y = 0.02$, the SAR significantly increased at $x = 0.5$. The Gd^{3+} ion has a higher effective magnetic moment than Fe^{3+} ion (Calderon-Ortiz et al. 2009; Kadam et al. 2016; Kumar et al. 2014). In the Gd-substituted Mg–Zn ferrites, Fe^{3+} ions in the B-site can be replaced with Gd^{3+} ions, which may increase the magnetization and coercivity. Thus, the SAR can vary depending on x, according to the similar mechanism to the case of $y = 0$. Furthermore, Gd substitution decreased the SAR, because the magnetization can decrease due to an

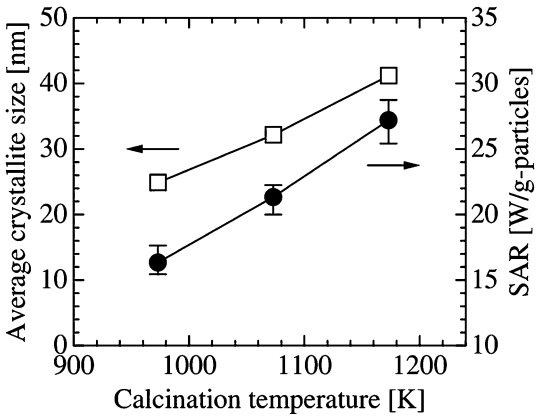

Fig. 7 Change in average crystallite size and SAR of $Mg_{0.5}Zn_{0.5}Gd_{0.02}Fe_{1.98}O_4$ with calcination temperature

Fe^{3+}–O–Fe^{3+} superexchange interaction in the ferrites (Calderon-Ortiz et al. 2009; Kadam et al. 2016). As Kadam et al. (2016) noticed, by replacing Fe^{3+} ions with Gd^{3+} ions, the valence state of iron on the B-site can change from Fe^{3+} (high spin $3d^5$) to Fe^{2+} (low spin $3d^6$), resulting in partial development of the Fe^{2+}–O–Fe^{3+} superexchange interaction, which is weaker than the Fe^{3+}–O–Fe^{3+} interaction. Accordingly, a magnetic dilution may occur due to the Gd substitution, resulting in a decrease in the SAR.

As shown in Fig. 7, when the calcination temperature of the $Mg_{0.5}Zn_{0.5}Gd_{0.02}Fe_{1.98}O_4$ sample was increased from 973 to 1173 K, the average crystallite size (indicated by open squares) increased from 24.9 to 41.2 nm due to the coalescence of small grains through the grain boundary diffusion during calcination (Caglar et al. 2009). This can increase the magnetization (Choodamani et al. 2014), resulting in an increase of the SAR with temperature, as indicated by closed circles.

In general, the induction heating properties of magnetic particles can be controlled by the particle diameter. For example, magnetite (Fe_3O_4) nanoparticles, which are widely used as the heating mediator with excellent induction heating properties, can exhibit the maximum heat dissipation under certain magnetic field conditions when the particle diameter is approximately 12 nm; however, a slight variation of the particle diameter can cause a drastic decrease of the heat dissipation (Jeyadevan 2010). Therefore, the particle size distribution must be precisely adjusted to obtain the appropriate induction heating properties (Murase et al. 2011). Although various methods for preparing the magnetic particles with different diameters have been proposed so far (Iljinas et al. 2005; Iwasaki et al. 2010; Jing et al. 2012; Mizutani et al. 2010; Nemati et al. 2017), it is hard to precisely adjust the particle size distribution, which may lead to insufficient control of the induction heating properties. In contrast, our results demonstrate that the induction heating properties of Gd-substituted Mg–Zn ferrites can be relatively easily controlled by the metal composition compared with the particle size. We believe that this is one of the advantages that the Gd-substituted Mg–Zn ferrite nanoparticles have over magnetic particles available for hyperthermia.

Conclusion

$Mg_xZn_{1-x}Gd_yFe_{2-y}O_4$ nanoparticles were prepared via coprecipitation of metal hydroxides, followed by calcination in the air. The synthesis process can successfully provide pure $Mg_xZn_{1-x}Gd_yFe_{2-y}O_4$ with x ranging from 0.25 to 0.75 and y ranging from 0 to 0.06, although some Gd-substituted Zn and Mg ferrites (i.e., $x = 0$ and 1) contain $GdFeO_3$ as a by-product. The lattice parameter and crystallite size were found to depend strongly on the composition, leading to a variation of the magnetic induction heating properties. The SAR values of the $Mg_xZn_{1-x}Fe_2O_4$ samples were at a maximum at $x = 0.75$. However, when Fe^{3+} ions were replaced with Gd^{3+} ions, i.e., at higher y values, the maximum SAR values were observed at $x = 0.5$ and decreased with y. The calcination temperature also significantly affected the SAR due to a variation of the crystallite size, which can alter the magnetization. We confirmed that the induction heating properties of Gd-substituted Mg–Zn ferrites can be relatively easily controlled by adjusting the metal composition. The results suggest that Gd-substituted Mg–Zn ferrite nanoparticles are a promising candidate for heating mediators used in magnetic hyperthermia treatments for cancer.

Acknowledgements This work was supported by JSPS KAKENHI Grant Number JP15K04625.

References

Ali IA, Mohamed GY, Azzam A, Sattar AA (2017) Determination of concentrations of Fe, Mg, and Zn in some ferrite samples using neutron activation analysis and X-ray fluorescence techniques. Appl Radiat Isotopes 122:63–67. doi:10.1016/j.apradiso.2017.01.009

Caglar Y, Ilican S, Caglar M, Yakuphanoglu F, Wu J, Gao K, Lu P, Xue D (2009) Influence of heat treatment on the nanocrystalline structure of ZnO film deposited on p-Si. J Alloys Compd 481:885–889. doi:10.1016/j.jallcom.2009.03.140

Calderon-Ortiz E, Perales-Perez O, Voyles P, Gutierrez G, Tomar MS (2009) $Mn_xZn_{1-x}Fe_{2-y}R_yO_4$ (R = Gd, Eu) ferrite nanocrystals

for magnetocaloric applications. Microelectron J 40:677–680. doi:10.1109/INTMAG.2006.375464

Chaudhary R, Kanwar RK, Kanwar JR (2015) Zinc ferrite nanoparticles as highly effective magnetic resonance imaging contrast agents with emphasis on atherosclerosis. J Nanomater Mol Nanotechnol 4:3. doi:10.4172/2324-8777.1000164

Choodamani C, Nagabhushana GP, Rudraswamy B, Chandrappa GT (2014) Thermal effect on magnetic properties of Mg–Zn ferrite nanoparticles. Mater Lett 116:227–230. doi:10.1016/j.matlet.2013.11.024

Choodamani C, Rudraswamy B, Chandrappa GT (2016) Structural, electrical, and magnetic properties of Zn substituted magnesium ferrite. Ceram Int 42:10565–10571. doi:10.1016/j.ceramint.2016.03.120

Elkady AS, Hussein SI, Rashad MM (2015) Structural and magnetic properties of Gd^{3+} ion substituted magnesium ferrite nanopowders. J Magn Magn Mater 385:70–76. doi:10.1016/j.jmmm.2015.03.008

El-Sayed HM, Ali IA, Azzam A, Sattar AA (2017) Influence of the magnetic dead layer thickness of Mg–Zn ferrites nanoparticle on their magnetic properties. J Magn Magn Mater 424:226–232. doi:10.1016/j.jmmm.2016.10.049

Gao J, Yan Z, Liu J, Zhang M, Guo M (2015) Synthesis, structure and magnetic properties of Zn substituted Ni–Co–Mn–Mg ferrites. Mater Lett 141:122–124. doi:10.1016/j.matlet.2014.11.062

Ghodake UR, Kambale RC, Suryavanshi SS (2017) Effect of Mn^{2+} substitution on structural, electrical transport and dielectric properties of Mg–Zn ferrites. Ceram Int 43:1129–1134. doi:10.1016/j.ceramint.2016.10.053

Hajarpour S, Gheisari K, Raouf AH (2013) Characterization of nanocrystalline $Mg_{0.6}Zn_{0.4}Fe_2O_4$ soft ferrites synthesized by glycine-nitrate combustion process. J Magn Magn Mater 329:165–169. doi:10.1016/j.jmmm.2012.10.023

Haralkar SJ, Kadam RH, More SS, Shirsath SE, Mane ML, Patil S, Mane DR (2012) Substitutional effect of Cr^{3+} ions on the properties of Mg–Zn ferrite nanoparticles. Physica B 407:4338–4346. doi:10.1016/j.physb.2012.07.030

Hejase HA, Hayek SS, Qadri SM, Haik YS (2012) Self-controlled hyperthermia characteristics of ZnGdFe nanoparticles. IEEE Trans Magn 48:2430–2439. doi:10.1109/TMAG.2012.2196284

Hirosawa F, Iwasaki T, Watano S (2016) Induction heating properties of Gd-substituted Mg–Zn ferrite nanoparticles in an AC magnetic field. In: Proceedings of 9th Pacific Rim international conference on advanced materials and processing (PRICM9), PS6-17

Iljinas A, Brucas R, Stankus V, Dudonis J (2005) Synthesis of Fe_3O_4 thin films by solid state reactions. Mater Sci Eng C 25:590–594. doi:10.1016/j.msec.2005.06.031

Iwasaki T, Mizutani N, Watano S, Yanagida T, Kawai T (2010) Size control of magnetite nanoparticles by organic solvent-free chemical coprecipitation at room temperature. J Exp Nanosci 5:251–262. doi:10.1080/17458080903490731

Jeyadevan B (2010) Present status and prospects of magnetite nanoparticles-based hyperthermia. J Ceram Soc Jpn 118:391–401. doi:10.2109/jcersj2.118.391

Jing J, Zhang Y, Liang J, Zhang Q, Bryant E, Avendano C, Colvin VL, Wang Y, Li W, Yu WW (2012) One-step reverse precipitation synthesis of water-dispersible superparamagnetic magnetite nanoparticles. J Nanopart Res 14:827–834. doi:10.1007/s11051-012-0827-3

Kadam RH, Desai K, Shinde VS, Hashim M, Shirsath SE (2016) Influence of Gd^{3+} ion substitution on the $MnCrFeO_4$ for their nanoparticle shape formation and magnetic properties. J Alloys Compd 657:487–494. doi:10.1016/j.jallcom.2015.10.164

Klemme S, Ahrens M (2005) Low-temperature heat capacity of magnesioferrite ($MgFe_2O_4$). Phys Chem Miner 32:374–378. doi:10.1007/s00269-005-0003-8

Kumar G, Shah J, Kotnala RK, Dhiman P, Rani R, Singh VP, Garg G, Shirsath SE, Batoo KM, Singh M (2014) Self-ignited synthesis of Mg–Gd–Mn nanoferrites and impact of cation distribution on the dielectric properties. Ceram Int 40:14509–14516. doi:10.1016/j.ceramint.2014.07.017

Mansour SF, Abdo MA (2017) Electrical modulus and dielectric behavior of Cr^{3+} substituted Mg–Zn nanoferrites. J Magn Magn Mater 428:300–305. doi:10.1016/j.jmmm.2016.12.039

Mizutani N, Iwasaki T, Watano S, Yanagida T, Kawai T (2010) Size control of magnetite nanoparticles in hydrothermal synthesis by coexistence of lactate and sulfate ions. Curr Appl Phys 10:801–806. doi:10.1016/j.cap.2009.09.018

Murase K, Oonoki J, Takata H, Song R, Angraini A, Ausanai P, Matsushita T (2011) Simulation and experimental studies on magnetic hyperthermia with use of superparamagnetic iron oxide nanoparticles. Radiol Phys Technol 4:194–202. doi:10.1007/s12194-011-0123-4

Nemati Z, Das R, Alonso J, Clements E, Phan MH, Srikanth H (2017) Iron oxide nanospheres and nanocubes for magnetic hyperthermia therapy: a comparative study. J Electron Mater. doi:10.1007/s11664-017-5347-6

Raja P, Yadavalli T, Ravi D, Therese HA, Ramasamy C, Hayakawa Y (2017) Synthesis and magnetic properties of gadolinium substituted zinc ferrites. Mater Lett 188:406–408. doi:10.1016/j.matlet.2016.11.083

Reyes-Rodríguez PY, Cortés-Hernández DA, Escobedo-Bocardo JC, Almanza-Robles JM, Sánchez-Fuentes HJ, Jasso-Terán A, León-Prado LED, Méndez-Nonell J, Hurtado-López GF (2017) Structural and magnetic properties of Mg–Zn ferrites ($Mg_{1-x}Zn_xFe_2O_4$) prepared by sol-gel method. J Magn Magn Mater 427:268–271. doi:10.1016/j.jmmm.2016.10.078

Sharma R, Thakur P, Kumar M, Thakur N, Negi NS, Sharma P, Sharma V (2016) Improvement in magnetic behaviour of cobalt doped magnesium zinc nano-ferrites via co-precipitation route. J Alloys Compd 684:569–581. doi:10.1016/j.jallcom.2016.05.200

Smolkova IS, Kazantseva NE, Parmar H, Babayan V, Smolka P, Saha P (2015) Correlation between coprecipitation reaction course and magneto-structural properties of iron oxide nanoparticles. Mater Chem Phys 155:178–190. doi:10.1016/j.matchemphys.2015.02.022

Yao A, Ai F, Wang D, Huang W, Zhang X (2009) Synthesis, characterization and in vitro cytotoxicity of self-regulating magnetic implant material for hyperthermia application. Mater Sci Eng C 29:2525–2529. doi:10.1016/j.msec.2009.07.021